J|A|C|S
ARTICLES
Published on Web 11/16/2002

Guanine of the Third Strand of C·G*G Triplex Serves as an Effective Hole Trap

Chikara Dohno, Kazuhiko Nakatani, and Isao Saito*

Contribution from the Department of Synthetic Chemistry and Biological Chemistry, Faculty of Engineering, Kyoto University, CREST, Japan Science and Technology Corporation (JST), Kyoto 606-8501, Japan

Received April 29, 2002. Revised Manuscript Received September 25, 2002

Abstract: We have examined the structural and electronic effects of the one-electron oxidation of the C·G*G triplex, where G is located in a quite different environment from the G of duplex DNA. Upon photoirradiation of an external photosensitizer (riboflavin) with the C·G*G triplex, oxidative DNA cleavage occurred exclusively at guanine repeat sequences in the third strand of triple helix DNA. Hole transport through the C·G*G triplex also occurred, resulting in selective cleavage at G in the third strand. Thus, the hole generated in the duplex can migrate to GGG in the third strand and is trapped exclusively at Gs in the third strand. These experimental results, together with molecular orbital calculations, suggest that the origin of the selective strand cleavage can be explained as follows: (i) guanine repeat sequences in the third strand are more easily oxidized than in duplex DNA and (ii) in their radical cation states, G of the third strand rapidly deprotonates and reacts with oxygen and/or water, leading to strand cleavage. These results indicate that the oxidative damage preferentially occurred at Gs of the third strand owing to thermodynamic and kinetic features of the one-electron oxidation of the C·G*G triplex.

Introduction

A guanine radical cation (hole) produced by one-electron oxidation of DNA by a photoexcited sensitizer,[1−5] metal oxidants,[6] and ionizing radiation[7] is known to migrate to remote guanines (G) through the DNA π-stack.[8,9] Water and/or oxygen can trap holes, eventually producing guanine-damaged sites that ultimately cause aging and mutation. Because hole migration through DNA competes with hole trapping, hole trapping is an extremely important process in determining the overall efficiency of hole migration from hole donor to acceptor.[2,10] Although the precise mechanisms for hole trapping and product formation are not yet fully understood, base sequences, base stacking, and accessibility of water and/or oxygen to the hole are believed to be the principal factors significantly affecting the site and efficiency of hole trapping. In B-form duplex DNA, hole trapping was selectively observed at sequences of Gs. Stacking of two or more Gs lowers the ionization potential (IP) compared with that of a single isolated G, making stacked G sites thermodynamically more favorable for hole trapping.[11−13] In contrast to duplex DNA, the hole could be trapped at all Gs without apparent sequence selectivity in single stranded DNA, possibly due to the weak base stacking and an almost equal accessibility of water and oxygen to all Gs.

The structural effects of hole trapping were further discussed on the triple helix DNA containing the pyrimidine·purine·pyrimidine (py·pu·py, C·G*C^+) motif,[14,15] where G is located in a quite different environment from duplex DNA in terms of base stacking, hydrogen bonding, and solvent accessibility. Guanines within the base triplet are reported to be less reactive than G in a Watson−Crick base pair, due to (i) the increased positive charge caused by C protonation, (ii) reduced solvent and oxygen accessibility, and (iii) the altered base stacking effect. In addition to the C·G*C^+ motif, the py·pu·pu motif (C·G*G) is also known to produce G-containing triple helix

* To whom correspondence should be addressed. E-mail: saito@sbchem.kyoto-u.ac.jp.

(1) For reviews, see: (a) Grinstaff, M. W. *Angew. Chem., Int. Ed. Engl.* **1999**, *38*, 3629−3635. (b) Holmlin, R. L.; Dandliker, P. J.; Barton, J. K. *Angew. Chem., Int. Ed. Engl.* **1997**, *36*, 2714−2730.
(2) (a) Giese, B.; Amaudrut, J.; Köhler, A. K.; Spormann, M.; Wessely, S. *Nature* **2001**, *412*, 318−320. (b) Giese, B.; Spichty, M. *Chem. Phys. Chem.* **2000**, *1*, 195−198. (c) Giese, B. *Acc. Chem. Res.* **2000**, *33*, 631−636.
(3) Lewis, F. D.; Letsinger, R. L.; Wasielewski, M. R. *Acc. Chem. Res.* **2001**, *34*, 159−170.
(4) Schuster, G. B. *Acc. Chem. Res.* **2000**, *33*, 253−260.
(5) (a) Nakatani, K.; Dohno, C.; Saito I. *J. Am. Chem. Soc.* **2000**, *122*, 5893−5894. (b) Nakatani, K.; Dohno, C.; Saito I. *J. Am. Chem. Soc.* **1999**, *121*, 10 854−10 855.
(6) Hall, D. B.; Holmlin, R. E.; Barton, J. K. *Nature* **1996**, *382*, 731−734.
(7) (a) Melvin, T.; Botchway, S.; Parker, A. W.; O'Neill, P. *J. Chem. Soc., Chem. Commun.* **1995**, 653−654. (b) Becker, D.; Sevilla, M. D. *Adv. Radiat. Biol.* **1993**, *17*, 121−180.
(8) Jortner, J.; Bixon, M.; Langenbacher, T.; Michael-Beyerle, M. E. *Proc. Natl. Acad. Sci. U.S.A.* **1998**, *95*, 12 759−12 765.
(9) Berlin, Y. A.; Burin, A. L.; Ratner, M. A. *J. Am. Chem. Soc.* **2000**, *122*, 10 903−10 909.
(10) Nakatani, K.; Dohno, C.; Saito I. *J. Am. Chem. Soc.* **2001**, *123*, 9681−9682.
(11) (a) Yoshioka, Y.; Kitagawa, Y.; Takano, Y.; Yamaguchi, K.; Nakamura, T.; Saito I. *J. Am. Chem. Soc.* **1999**, *121*, 8712−8719. (b) Saito, I.; Nakamura, T.; Nakatani, K.; Yoshioka, Y.; Yamaguchi, K.; Sugiyama, H. *J. Am. Chem. Soc.* **1998**, *120*, 12 686−12 687. (c) Sugiyama, H.; Saito, I. *J. Am. Chem. Soc.* **1996**, *118*, 7063−7068.
(12) Voityuk, A. A.; Jortner, J.; Bixon, M.; Rösch, N. *Chem. Phys. Lett.* **2000**, *324*, 430−434.
(13) Prat, F.; Houk, K. N.; Foote, C. S. *J. Am. Chem. Soc.* **1998**, *120*, 845−846.
(14) Kan, Y.; Schuster, G. B. *J. Am. Chem. Soc.* **1999**, *121*, 11 607−11 614.
(15) Núñez, M. E.; Noyes, K. T.; Gianolio, D. A.; McLaughlin, L. W.; Barton, J. K. *Biochemistry* **2000**, *39*, 6190−6199.

10.1021/ja026724n CCC: $22.00

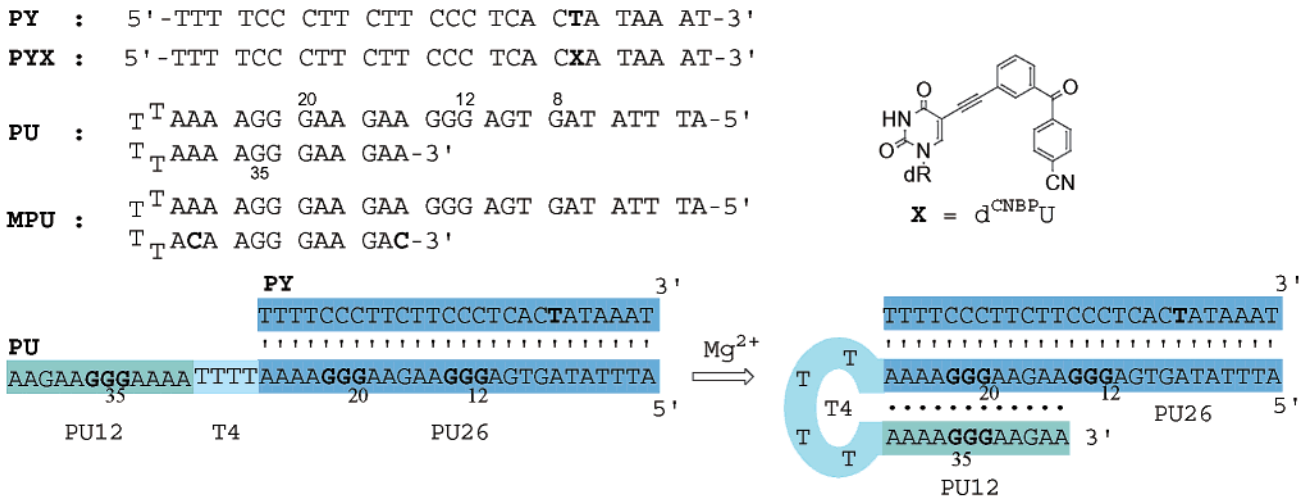

Figure 1. ODNs used in this study and schematic illustration of intramolecular triplex motif. **PU** consists of three segments, PU12, T4, and PU26. The formation of the C·G*G triplex is accelerated by the presence of multivalent cations. X denotes $d^{CNBP}U$.

DNAs. Although all triples in the py·pu·pu triplex are noniso-morphous and tend to be less stable than the py·pu·py triplex, the py·pu·pu triplex has an obvious advantage in that the triplex can be formed at physiological pH in the presence of Mg^{2+} ion.[16] A more frequent type of C·G*G triplex motif involves Gs of the third strand bound antiparallel to the Watson−Crick purine strand by reversed Hoogsteen hydrogen bonding. Structural studies have revealed that the binding of the third strand displaces the base pairs in the duplex toward the minor groove, while unwinding the helix.[17] The guanines adopt anti glycosidic torsion angles and S-type sugar puckerings. On the basis of these structural features, the C·G*G triplex is anticipated to have different physical and chemical properties for both hole transport and trapping.

We herein report that a hole produced at G in a Watson−Crick base pair was selectively trapped at the G of the third strand of a C·G*G triplex. Molecular orbital calculations on the neutral and radical cation of C·G*G suggest that hole trapping at the G of the third strand is thermodynamically and kinetically more favorable.

Results and Discussion

Design and Characterization of C·G*G Triplex DNA. We employed a 26-mer pyrimidine-rich strand (**PY** and **PYX**) and a 42-mer purine-rich probe strand (**PU** and **MPU**). **PY** and **PYX** contain a continuous pyrimidine sequence on their 5′-end, whereas **PU** consists of three segments, (1) a 26-mer fully complementary sequence to **PY** (PU26), (2) a T4 loop sequence (T4) and (3) a 12-mer continuous purine sequence at the 3′-end (PU12). Hybridization of **PY**s and **PU** produces a 26-mer duplex with an overhang at the 3′-end consisting of T4 and PU12 segments. In the presence of Mg^{2+}, the PU12 region folds back along the major group of the duplex with reversed Hoogsteen hydrogen bonds, producing a 12-mer sequence of intramolecular py·pu·pu triplex. On the other hand, oligodeoxynucleotide **MPU** cannot form a stable intrramolecular triplex because mismatched base pairs are introduced in the 3′-end purine rich sequence. For studying hole transport through the C·G*G triplex, we used oligodeoxynucleotide **PYX**, which contains cyanobenzophenone substituted 2′-deoxyuridine ($d^{CNBP}U$)[5,18] as an electron accepting nucleobase instead of thymidine in **PY**. The hybrid **PY**/**PU** contains three distinct types of GGG sites, namely $G_{12}GG$ in the duplex region, $G_{20}GG$ in the Watson−Crick purine strand of the triplex region, and $G_{35}GG$ in the third strand of the triplex.

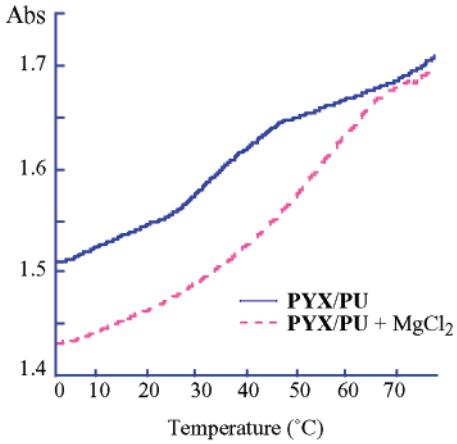

Figure 2. UV melting curves measured at 260 nm for **PYX**/**PU** (50 μM base concentration for each strand) in the presence of 2 mM $MgCl_2$ (dotted line) and in the absence of $MgCl_2$ (solid line) in 10 mM sodium cacodylate buffer (pH 7.0).

To confirm the formation of an intramolecular triple helix in the presence of $MgCl_2$, we carried out melting curve and circular dichroism (CD) measurements of **PYX**/**PU** in the presence and absence of $MgCl_2$. The thermal denaturation profiles of **PYX**/**PU** with and without 2 mM $MgCl_2$ are shown in Figure 2. In the absence of $MgCl_2$, the temperature corresponding to the melting of the 26-mer duplex was determined to be 44 °C. In the presence of $MgCl_2$, the melting curve shifted to higher temperature without the appearance of a distinct transition from duplex to triplex. The observed diffuse monophasic transition from triple to random coil is in good agreement with previous studies reported for the C·G*G triplex.[19] In the CD spectra, both positive and negative bands at 273 and 247 nm increased in

(16) (a) Thuong, N. T.; Hélène, C. *Angew. Chem., Int. Ed. Engl.* **1993**, *32*, 666−690. (b) Beal, P. A.; Dervan, P. B. *Science* **1991**, *251*, 1360−1363. (c) Kowhi, Y.; Kowhi-Shigematsu, T. *Proc. Natl. Acad. Sci. U.S.A.* **1988**, *85*, 3781−3785.

(17) (a) Radhakrishnan, I.; Patel, J. D. *Structure* **1993**, *1*, 135−152. (b) Radhakrishnan, I.; de los Santos, C.; Patel, J. D. *J. Mol. Biol.* **1991**, *221*, 1403−1418.

(18) Nakatani, K.; Dohno, C.; Saito I. *J. Org. Chem.* **1999**, *64*, 6901−6904.

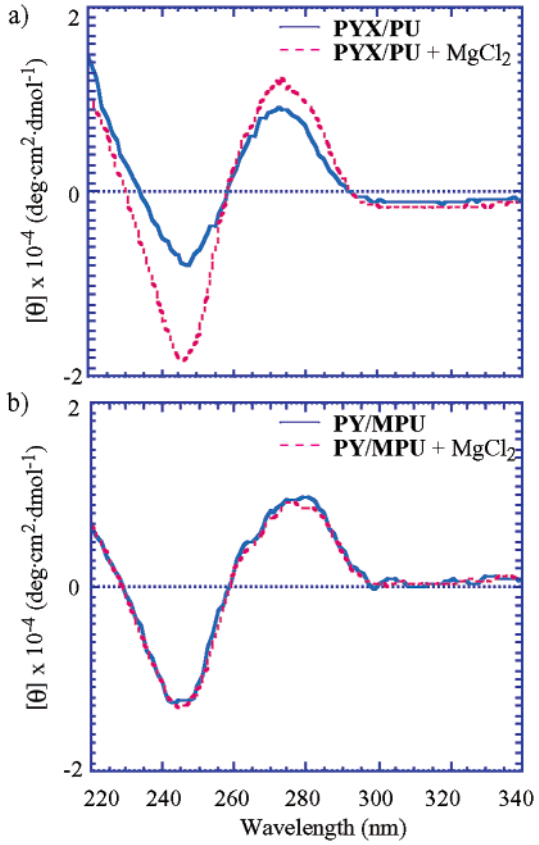

Figure 3. CD spectra of (a) **PYX**/**PU** and (b) **PY**/**MPU**. Dotted lines show CD spectra in the presence of 2 mM $MgCl_2$ and solid lines show without $MgCl_2$.

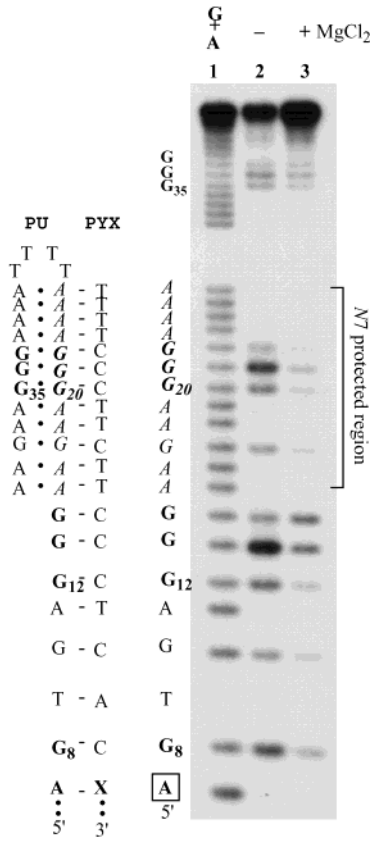

Figure 4. Autoradiograms of a denaturing sequencing gel for footprinting with DMS of **PYX**/**PU** in the presence and absence of $MgCl_2$. The ^{32}P-5′ end labeled **PU** was hybridized to the complementary strands **PYX** (2 μM, strand concentration) in 10 mM sodium cacodylate at pH 7.0. The hybridized ODNs were treated with DMS under the conditions in the Experimental Section. Lane 1, Maxam−Gilbert G+A sequencing reactions: lane 2, DMS footprinting assay performed in the absence of $MgCl_2$; lane 3, in the presence of 2 mM $MgCl_2$. The partial sequence of **PU** is shown on the left side of the gel.

intensity in the presence of $MgCl_2$ (Figure 3a). This observation is consistent with those previously reported.[19] In contrast, no marked change was observed in the CD spectra of mismatched triplex **PY**/**MPU** (Figure 3b). These results indicate that the structural change in the presence of $MgCl_2$ is attributable to the triplex formation.

Formation of a C·G*G triplex was further confirmed by the dimethyl sulfate (DMS) footprinting technique. DMS reacts predominantly at the N7-position of guanine in the B-form duplex. In a C·G*G triplex, the N7-position of guanine in the Watson−Crick duplex (G_{20}GG) is involved in reversed Hoogsteen hydrogen bonding to guanine in the third strand and, consequently, is protected from DMS alkylation.[20] The results of DMS footprinting are shown in Figure 4. In the absence of $MgCl_2$, strand cleavage occurred at all guanines with intrinsic sequence selectivity (lane 2). In marked contrast, cleavage at the G_{20}GG triplet was dramatically suppressed in the presence of $MgCl_2$, although cleavage at other G triplet sites became somewhat weaker (lane 3). Protection of G_{20}GG from DMS alkylation clearly indicated the formation of the C·G*G triplex in the presence of $MgCl_2$.

Photooxidation of the C·G*G Triplex by Riboflavin. We first examined the one-electron oxidation of **PY**/**PU** with the external photosensitizer riboflavin (Figure 5a). In the absence of $MgCl_2$, selective cleavages were observed at all three G triplets (lane 2). Although both the G_{12}GG and the G_{20}GG triplets are located in the duplex and the G_{35}GG triplet is in a single strand region, no significant difference in the cleavage intensity was observed. The 5′-side and central Gs in G_{12}GG and G_{20}GG are major cleavage sites in the duplex region (lane 2). These observations are fully consistent with previous reports.[11a,21,22] In the presence of $MgCl_2$, the cleavage efficiency at G_{12}GG and G_{20}GG dramatically decreased with concomitant increase in the intensity at G_{35}GG (lane 1). Under these conditions, more than 90% of the cleavage is localized on G_{35}GG of the third strand of the C·G*G triplex region. The strong cleavage band of G_{35}GG is selective at the 5′-side and central Gs, and only weak cleavage was detected at the 3′-side G. The observed 5′-side selectivity for the G triplet implies that the GG stacking interaction is still valid for the specific cleavage in the third strand of the C·G*G triplex.

The photooxidation of **PY**/**PU** showed that the G triplet in the third strand of the C·G*G triplex is the exclusive site for formation of a piperidine-labile product when a hole was randomly generated on **PY**/**PU** by an external photosensitizer. The efficiency of hole trapping at this G triplet relative to that

(19) (a) Gondeau, C.; Maurizot, J. C.; Durand, M. *Nucleic. Acids. Res.* **1998**, *26*, 4996−5003. (b) Chen, F. M. *Biochemistry* **1991**, *30*, 4472−4479. (c) Pilch, D. S.; Levenson, C.; Shafer, R. H. *Biochemistry* **1991**, *30*, 6081−6087.

(20) (a) Balatskaya, S. V.; Belotserkovskii, B. P.; Johnston, B. H. *Biochemistry* **1996**, *35*, 13 328−13 337. (b) Voloshin, O. N.; Mirkin, S. M.; Lyamichev, V. I.; Belotserkovskii, B. P.; Frank-Kamenetskii, M. D. *Nature* **1988**, *333*, 475−476.

(21) Burrows, C. J.; Muller, J. G. *Chem. Rev.* **1998**, *98*, 1109−1151.

(22) Zhu, Q.; LeBreton, P. R. *J. Am. Chem. Soc.* **2000**, *122*, 12 824−12 834.

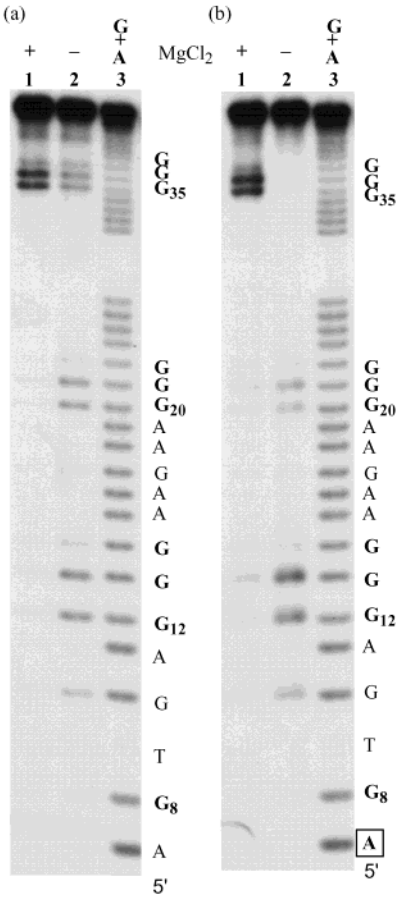

Figure 5. Autoradiograms of a denaturing sequencing gel for oxidation of C·G*G triplex by external and internal oxidants. (a) Photoreactions of ODN **PYX**/**PU** which contained internal oxidant, ^{CNBP}U (X). The ^{32}P-5′ end labeled **PU** was hybridized to th ecomplementary strands (2 μM, strand concentration) and the hybridized ODNs were irradiaded with a transilluminator under the conditions as described in Experimental Section. Lane 1, photoirradiation for 30 min in the presence of $MgCl_2$; lane 2 photoirradiation for 60 min in the absence of $MgCl_2$; lane 3, Maxam−Gilbert G+A sequencing reactions. d^{CNBP}U is located opposite to the A shown with a box.

in a Watson−Crick duplex was further investigated using **PYX** containing an internal photosensitizer, d^{CNBP}U.

Hole Trap at the Guanines in the Third Strand. Upon photoirradiation of the duplex containing d^{CNBP}U (**PYX**/**PU**), a guanine radical cation was site-selectively generated at G_8 by a single electron transfer to a proximal photoexcited d^{CNBP}U.[5] In this system, we can assess the contribution of DNA-mediated hole transport to the selective cleavage observed in the "external" oxidant, riboflavin. The pattern of strand cleavage shown in Figure 5b (lane 2) was nearly the same as in Figure 5a (lane 2) (Figure 6). The only difference in the cleavage pattern for riboflavin and d^{CNBP}U was GGG_{35} cleavage, which was not observed in the absence of $MgCl_2$ (Figure 5b, lane 2). Hole transfer to GGG_{35} could not occur through a long single strand bridge between GGG_{20} and GGG_{35}, which would be a poor π-stacked medium. In the presence of $MgCl_2$, the hole generated at G_8 migrated through the double stranded DNA and reached GGG_{35} in the third strand via an interstrand hole transfer (Figure 5b, lane 2). These results clearly indicate that hole transport is responsible for the selective cleavage at GGG_{35}, and GGG in the third strand acts as a more effective hole trap than GGG in the double strand. Although it has previously been reported that a charge moves through the py·pu·py triplex region to the duplex,[14,15,23] this is the first example that shows that the hole can migrate into the third strand.

Theoretical Analysis of the Oxidation of the C·G*G Triplex: C·G*G as a Thermodynamic Sink. Guanine repeat sequences are the hot spots for DNA damage by one-electron oxidation in B-form DNA. Several years ago, we demonstrated both experimentally and by ab initio molecular orbital calculation that 5′-*GG*-3′ and 5′-*GGG*-3′ (the italicized bases are the principal sites of cleavage) in B-form DNA are most easily oxidized due to the GG stacks and can act as thermodynamic sinks in DNA-mediated hole transport.[11] To elucidate the origin of the specific cleavage in the third strand of the C·G*G triplex, we performed molecular orbital calculations on the C·G*G triplex. For simplicity, $d(C{\cdot}G{*}G)_2$ was chosen for the calculations and its geometry was obtained from the NMR minimized average structure of the intramolecular C·G*G triplex 5′-TCC TCC TTT TTT AGG AGG ATT TTT TGG TGG T-3′.[17a] All of the sugar backbones were then replaced by methyl groups, keeping the position of all atoms fixed. Calculations were carried out at the B3LYP/6-31G level using the Gaussian 94 program package.[24] The calculated ionization potential (IP) of $d(C{\cdot}G{*}G)_2$ estimated by Koopmans' theorem is 3.96 eV, which is lower than that of the duplex 5′-CCC-3′/5′-GGG-3′ (4.17 eV). Such a low IP value of $d(C{\cdot}G{*}G)_2$ obtained by this calculation would be an underestimate;[25] however, the result at least indicates that $d(C{\cdot}G{*}G)_2$ is more easily oxidized and can act as a more effective thermodynamic sink than the GGG triplet in duplex DNA. It is also noteworthy that almost all of the highest occupied molecular orbital (HOMO) of $d(C{\cdot}G{*}G)_2$ is concentrated on the 5′-G of GG in the third strand (Figure 7). These calculations indicate the 5′-G of GG in the third strand is the most electron donating site in $d(C{\cdot}G{*}G)_2$.

C·G*G as a Kinetic Hole Trap. The calculated radical cation state of the C·G*G triple provided significant information regarding the selective cleavage at guanines in the third strand. The geometries of ground-state C·G*G and radical cation state $(C{\cdot}G{*}G)^{\bullet+}$ were optimized at the B3LYP/3-21G level. Figure 8 shows the optimized structure of $(C_1{\cdot}G_1{*}G_2)^{\bullet+}$ superimposed on $C_1{\cdot}G_1{*}G_2$. The differences in the hydrogen bond lengths between neutral and radical cation states of $C_1{\cdot}G_1{*}G_2$ are summarized in Table 1. The major points in Table 1 are as follows: (i) the bond length of N1−H (G_2) increased by 0.09 Å and (ii) the distance between N1 (G_2) proton and N7 (G_1) decreased by 0.21 Å in the radical cation state. It is conceivable that this proton shift from N1 (G_2) to N7 (G_1) caused the acceleration of deprotonation of G_2 in $(C_1{\cdot}G_1{*}G_2)^{\bullet+}$. On the other hand, the proton shift from N1 (G_1) to N3 (C_1) is much smaller than the shift N1 (G_2) to N7 (G_1). The ease of deprotonation from G_2, not from G_1, is critical for the selective

(23) Lewis, F. D.; Wu, Y.; Hayes, R. T.; Wasielewski, M. R. *Angew. Chem., Int. Ed.* **2002**, *41*, 3485−3487.
(24) Frisch, M. J.; Trucks, G. W.; Schlegel, H. B.; Gill, P. M. W.; Johnson, B. G.; Robb, M. A.; Cheeseman, J. R.; Keith, T. A.; Petersson, G. A.; Montgomery, J. A.; Raghavachari, K.; Al-Laham, M. A.; Zakrzewski, V. G.; Oritiz, J. V.; Foresman, J. B.; Cioslowski, J.; Stefanov, B. B.; Nanayakkara, A.; Challacombe, M.; Peng, C. Y.; Ayala, P. Y.; Chen, W.; Wong, M. W.; Andres, J. L.; Replogle, E. S.; Gomperts, R.; Martin, R. L.; Fox, D. J.; Binkley, J. S.; Defrees, D. J.; Baker, J.; Stewart, J. P.; Head-Gordon, M.; Gonzalez, C.; Pople, J. A. *Gaussian 94*; Gaussian, Inc.: Pittsburgh, PA, 1995.
(25) Recently, several experimental results suggested GG and GGG are shallow hole trap and these IPs are considerably higher than our previous calculations.[12,26]

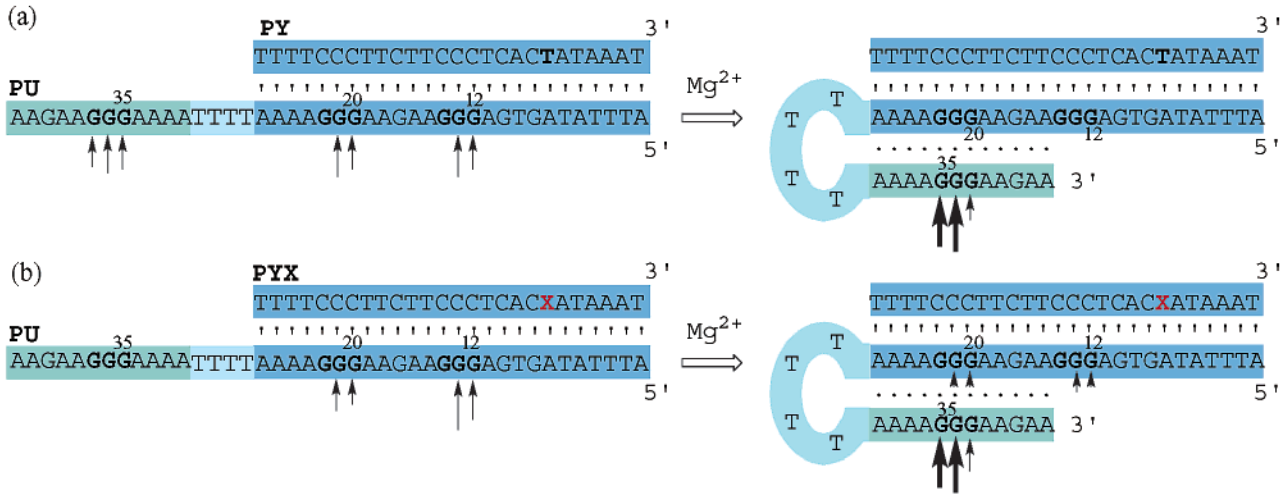

Figure 6. Schematic representation of the cleavage patterns in the duplex (a) **PY**/**PU** and (b) **PYX**/**PU**. The arrows indicate the cleavage sites and their relative efficiency.

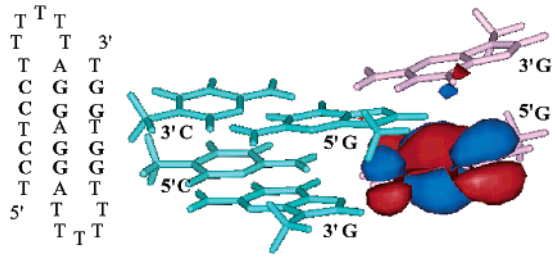

Figure 7. Orbital contour plot of the HOMO of d(C·G*G)$_2$ obtained by density functional calculation using GAUSSIAN 94 at the B3LYP/6-31G level. The geometry was obtained from NMR of 31-mer intramolecular triplex (left). Almost all of the HOMO is concentrated on 5′-G of GG in the third strand.

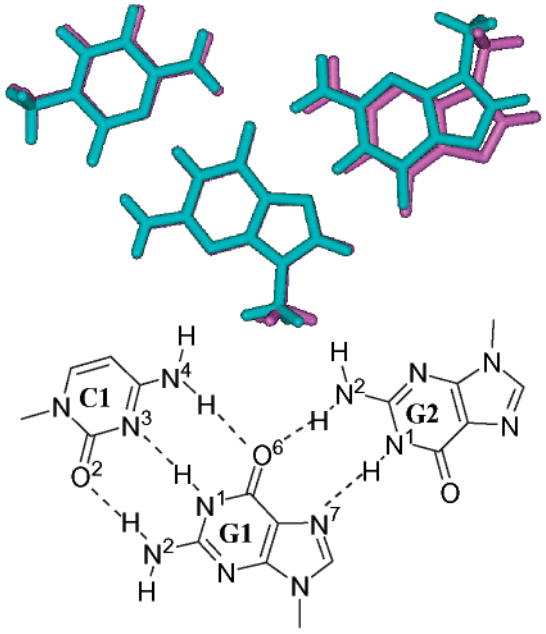

Figure 8. View of (C·G*G)$^{\bullet+}$ (cyan) superposed on C·G*G triplet (magenta). The geometries were optimized at the Becke3LYP/3-21G level utilizing Gaussian94 and Spartan program.

cleavage on the third strand, because deprotonation of the guanine radical cation is considered to be the first step leading to alkali labile products.[27,28]

Table 1. Difference of the Calculated Hydrogen Bond Lengths (Δ) between Neutral and Radical Cation State of C·G*G Triplet[a,b]

hydrogen bonds	neutral	radical cation	Δ
G_1-C_1 O^6-HN^4	1.695	1.760	0.065
	(1.051)	(1.039)	(−0.012)
N^1H-N^3	(1.057)	(1.070)	(0.013)
	1.762	1.739	−0.023
N^2H-O^2	(1.036)	(1.044)	(+0.008)
	1.753	1.678	−0.078
G_1-G_2 N^7-HN^1	1.655	1.442	−0.213
	(1.055)	(1.149)	(+0.094)
O^6-HN^2	2.012	1.668	−0.344
	(1.025)	1.058)	(+0.033)

[a] The lengths (Å) were obtained from optimized structure at B3LYP/3-21G. [b] The lengths of covalent N−H bonds in parentheses.

Although the pK_a of the guanine radical cation (pK_a = 3.9) is more acidic than that of guanine itself (pK_a = 9.4) and N3-protonated cytosine (pK_a = 4.3),[21,29] the proton shift from N1 (G_1) to N3 (C_1) in (C_1·G_1*G_2)$^{\bullet+}$ was negligibly small according to this calculation (Table 1).[30] It is, therefore, reasonable to assume that (C_1·G_1*G_2)$^{\bullet+}$ behaves like C_1·G_1*(G_2)$^{\bullet+}$. This speculation was further supported by the spin density map (Figure 9). The spin densities of the optimized (C_1·G_1*G_2)$^{\bullet+}$ are completely localized on G_2. The G_2 in (C_1·G_1*G_2)$^{\bullet+}$, which has an exclusively oxidized character, can rapidly deprotonate and undergo subsequent reactions with oxygen and/or water. Taken together, these calculations strongly support the conclusion that hole trapping preferentially occurred at Gs in the third strand.

Conclusions

The experimental results reported here provide new "hot spots" for oxidative damage in DNA. The oxidative DNA

(26) (a) Lewis, F. D.; Wu, T.; Liu, X.; Liu, J.; Hayes, R. T.; Wasielewski, M. R. *J. Am. Chem. Soc.* **2000**, *122*, 12 037−12 038. (b) Davis, W. B.; Naydenova, I.; Haselsberger, R.; Ogrodnik, A.; Giese, B.; Michel-Beyerle, M. E. *Angew. Chem., Int. Ed.* **2000**, *39*, 3649−3652.
(27) Cadet, J.; Berger, M.; Buchko, G. W.; Joshi, P. C.; Raoul, S.; Ravanat, J. L. *J. Am. Chem. Soc.* **1994**, *116*, 7403−7404.
(28) The mechanism of hole trapping where guanine radical cation is irreversibly converted to alkali labile sites is rather complicated and poorly understood.[21] The hydration of guanine radical cation is also considered to be responsible for hole trapping process in duplex DNA.
(29) Steenken, S. *Biol. Chem.* **1997**, *378*, 1293−1297.
(30) The proton shift from N1 of guanine to N3 cytosine in the (C·G)$^{\bullet+}$ has been confirmed by *ab initio* and density functional calculations. Hutter, M.; Clark, T. *J. Am. Chem. Soc.* **1996**, *118*, 7574−7577.

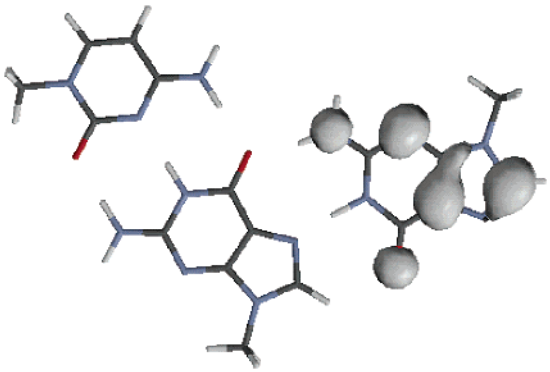

Figure 9. Spin densities of the optimized $(C{\cdot}G{*}G)^{\bullet+}$. In optimized structure, almost all of the spin densities are localized on G in the third strand.

cleavage occurred exclusively at guanine repeat sequences in the third strand of triple helix DNA. Molecular orbital calculations suggest the following: (i) guanine repeat sequences in the third strand are more easily oxidized than in duplex DNA and (ii) in their radical cation states, G in the third strand rapidly deprotonates and reacts with oxygen and/or water, leading to strand cleavage. A hole generated in the duplex can migrate to GGG in the third strand and is trapped exclusively at Gs in the third strand for both thermodynamic and kinetic reasons.

Experimental Section

Materials. The reagents for the DNA synthesis were purchased from Glen Research. Calf intestine alkaline phosphatase (AP), snake venom phosphodiesterase (s.v. PDE), and Nuclease P1 were purchased from Boehringer Manheim. Riboflavin was purchased from Nacalai Tesque Co. Ltd. The oligodeoxynucleotides (ODN) **PY** and **PU** were purchased from Amersham Pharmacia Biotech. T4 kinase was purchased from NIPPON GENE (10 units/μL), and [γ-^{32}P]-ATP (10 mCi/mL) was from Amersham Pharmacia Biotech. All aqueous solutions utilized purified water (Millipore, Milli-Q sp UF).

Oligonucleotides Synthesis and Purification. Automated DNA synthesis was carried out by using a standard β-(cyanoethyl)phosphoramidite method with Applied Biosystems 392 DNA synthesizer. The coupling of $d^{CNBP}U$ phosphoramidite[18] was conducted as usual except for the coupling time of 15 min. Synthesized ODN were deprotected and removed from the solid support by treating with concentrated ammonia at 37 °C for 24 h. Purification of the ODNs was performed on a CHEMCOBOND 5-ODS−H HPLC column with a linear gradient of 5−20% acetonitrile in 100 mM triethylammonium acetate for 30 min at a flow rate 3.0 mL/min. The purified ODNs were characterized by matrix-assisted laser desorption ionization time-of-flight (MALDI-TOF) mass spectrometry. The purity and concentration of the synthesized ODNs was determined by complete digestion with s.v. PDE (0.15 units/mL), AP (50 units /mL), and nuclease P1 (50 units /mL) to 2′-deoxymononucleosides at 37 °C for 2 h.

Melting-Temperature (T_m) and Circular Dichroism (CD) Spectra Measurement. ODN solutions (50 μM, base concentration for each ODN strand) were prepared with 10 mM sodium cacodylate (pH 7.0) and either 2 mM $MgCl_2$ or no $MgCl_2$. Absorbance vs temperature profiles were measured at 260 nm using a JASCO V-550 UV/vis spectrometer connected with a JASCO TPU-436 temperature controller. The absorbance of the samples was monitored at 260 nm from 2 °C to 80 °C with a heating rate of 1 °C/min. The T_m value was determined as the maximum in a plot of $\Delta A260/\Delta T$ versus temperature. CD spectra were recorded on a JASCO J-770 instrument with the use of the same ODN solutions from 220 to 340 nm at 4 °C.

PAGE Analysis of Oxidative Cleavage of the Triplex by Photoexcited Riboflavin. The ODN **PU** (400 pmol-strand) was 5′-end-labeled by phosphorylation with 4 μL of [γ -^{32}P]-ATP and 4 μL of T4 polynucleotide kinase using standard procedures.[31a,b] The 5′-end-labeled ODN was recovered by ethanol precipitation and further purified by 15% denaturing gel electrophoresis, and isolated by the crush-and-soak method.[31c] The 5′-^{32}P-end labeled and cold ODN **PU** (<50 nM and 1 μM strand concentration, respectively) was hybridized to its complementary strand **PY** (1 μM) in 10 mM Na cacodylate buffer (pH 7.0) in the presence or absence of 2 mM $MgCl_2$. Hybridization was achieved by heating the sample at 90 °C for 3 min and slowly cooling to room temperature. The 5′-^{32}P-end-labeled ODN duplex (2.0×10^4 cpm) containing riboflavin (50 μM) was irradiated at 366 nm with a transilluminator at 4 °C for 30 min (in the presence of 2 mM $MgCl_2$) or 60 min (in the absence of $MgCl_2$). After irradiation, all reaction mixtures were ethanol-precipitated with the addition of 10 μL of 3 M sodium acetate, 10 μL of 10 μM calf thymus DNA, and 800 μL of cold ethanol. The precipitated DNA was washed with 100 μL of 80% cold ethanol and dried in vacuo. The dried DNA was dissolved in 10% piperidine (v/v), heated at 90 °C for 20 min, evaporated by vacuum rotary evaporation to dryness, and resuspended in 80% formamide loading buffer (a solution of 80% v/v formamide, 1 mM EDTA, 0.1% xylene cyanol, and 0.1% bromophenol blue). All reactions, along with Maxam−Gilbert G+A sequencing marker,[32] were heat denatured at 90 °C for 2 min and quickly chilled on ice. The samples (1 μL, 2×10^3 cpm) were loaded onto 15% polyacrylamide/7 M urea sequencing gels and electrophoresed at 1900 V for approximately 2 h.[33] The gel was transferred to a cassette and exposed to Fuji X-ray film (RX-U) with intensifying sheet at −80 °C. Cleavage of the labeled strand was quantified by phosphorimagery using Molecular Analyst software (version 2.1).

PAGE Analysis of Oxidative Cleavage of the Triplex Containing $d^{CNBP}U$. 5′-^{32}P-end labeled and cold ODN **PU** (<50 nM and 1 μM strand, respectively) was hybridized to its complementary strand **PYX** (1 μM) in 10 mM Na cacodylate buffer (pH 7.0) in the presence or absence of 2 mM $MgCl_2$. Hybridization was achieved by heating the sample at 90 °C for 3 min and slowly cooling to room temperature. The 5′-^{32}P-end-labeled ODN duplex (2.0×10^4 cpm) was irradiated at 312 nm with a transilluminator at 4 °C for 30 min (in the presence of 2 mM $MgCl_2$) or 60 min (in the absence of $MgCl_2$). Following procedure was the same as described in the preceding PAGE analysis experiment.

DMS Footprinting.[20,32] 5′-^{32}P-end labeled and cold ODN **PU** (<50 nM and 1 μM strand concentration, respectively) was hybridized to its complementary strand **PYX** (1 μM) in 10 mM Na cacodylate buffer (pH 7.0) in the presence or absence of 2 mM $MgCl_2$. Hybridization was achieved by heating the sample at 90 °C for 3 min and slowly cooling to room temperature. The hybridized ODNs containing DMS (10 mM) were allowed to stand for 3 min (in the absence of $MgCl_2$) or 6 min (in the presence of $MgCl_2$) at 0 °C. The reaction was quenched by adding 1 M C_2H_5SH, 10 μg/mL Herring Sperm DNA, and 1.5 M NaOAc (pH = 7.0). The DNA samples were then subjected to ethanol precipitation. After piperidine treatment (90 °C, 20 min), the samples were suspended in denaturing loading buffer and electrophoresed through a denaturing 15% polyacrylamide/7 M urea gel.

JA026724N

(31) (a) Maxam, A. M.; Gilbert, W. *Proc. Natl. Acad. Sci. U.S.A.* **1977**, *74*, 560−564. (b) Maniatis, T.; Fritsch, E. F.; Sambrook, J. *Molecular Cloning*; Cold Spring Harbor Laboratory Press: Plainview, New York, 1982. (c) Sambrook, J.; Fritsch, E. F.; Maniatis, T. *Molecular Cloning: A Laboratory Manual*, 2nd ed; Cold Spring Harbor Laboratory Press: Plainview, New York, 1989.
(32) Maxam, A. M.; Gilbert, W. *Methods Enzymol.* **1980**, *65*, 499−560.
(33) (a) Rickwood, D.; Hames, B. D. *Gel Electrophoresis of Nucleic Acids: A Practical Approach*, 2nd ed; IRL Press: New York, 1990. (b) Brown, T. A. *DNA Sequencing: The Basics*; IRL Press: New York, 1994.